19th Brazilian Congress of Thermal Sciences and Engineering
November 6th–10th, 2022, Bento Gonçalves - RS - Brazil

ENC-2022-0635
MATHEMATICAL MODEL FOR PROPELLANT GRAIN GEOMETRY REGRESSION

Leib de Andrade Neubarth
Rachel Lucena
Norberto Mangiavacchi
Daniel José Nahid Mansur Chalhub
Gil Roberto V. Pinheiro
José da Rocha Miranda Pontes
Rio de Janeiro State University, Rio de Janeiro, RJ, Brazil
leib999@yahoo.com.br, rachel.lucena@gmail.com, norberto.mangiavacchi@eng.uerj.br
daniel.chalhub@eng.uerj.br, gilpinheiro@eng.uerj.br, pontes.jose@gmail.com

Mauricio Ferrapontoff Lemos
Brazilian Navy Research Institute (IPqM), Rio de Janeiro, Brazil
engmlemos@gmail.com

Laurílio José da Silva Júnior
Empresa Gerencial de Projetos Navais (EMGEPRON), Rio de Janeiro, Brazil
laurilio.jr@gmail.com

Abstract. *Both in solid rocket engines and in gas generators (base bleed systems), the burning of a solid propellant - the grain - is the principle for gas generation. In these devices, the mass flow rate of gas generation is directly proportional to the surface area on which the combustion chemical reactions are taking place, depending on the surface of exposed propellant in the combustion chamber. Therefore, the geometry adopted by these grains is an important element of their performance, which is measured through the mass flow rate vs time curve. In this work, a mathematical model and the correspondent computational method will be presented, to describe and predict how the geometry, and the exposed surface of a grain deflagrates over time. The devised method consists in describing the grain surface, during the deflagration, as an unstructured mesh. Each time step, unitary vectors normal to the surface are calculated. These vectors are used to compute the directions taken by the moving points. The amount of displacement is given by the regression rate, obtained from experimental data. Despite being capable of predict the mesh evolution in a straightforward manner, two issues may appear during the simulation. First: two non-planar surfaces with normal pointing to each other can cause point/surface overlapping. And second, the distance between the points can become so small that numerical errors arise. The first problem is addressed through the elimination of some points, which smooths the surface. The criterion for deletion is based on the normals of the point's adjacent surfaces. When the internal product between such vectors is negative, it means that the angle between the surfaces is smaller than 90 degree. So, the point at the intersection is deleted. The second problem is solved using a contour parameterization. This allows the surface to be interpolated in order to achieve a more homogeneous distance between each point. This combined approach is able to simulate consistently the surface area vs time evolution, which reflects the measured mass flow rate vs time curve.*
Keywords: *base bleed, solid fuel regression, burn rate, geometrical modeling, numerical simulation*

1. INTRODUCTION

The base bleed is a system designed to increase the range of munitions. It does so by creating a gas discharge at the rear of the munition, reducing the pressure gradient between the front and rear. This reduces the aerodynamic drag, which in turn increases the range. (Lemos *et al.*, 2017)

Base bleed performance is tied to the mass flow of combustion products during its functioning. One approach to quantify such flow is calculating the grain surface exposed to combustion and the regression rate normal to this surface. The former can be obtained through geometrical modelling of the grain and the latter by correlations. Such approach is

disclosed in (Sutton and Biblarz, 2016) and given by

$$\dot{m}(t) = A\, r\, \rho, \tag{1}$$

where A is the surface area, r the regression rate and ρ the grain density. The density is constant through the base bleed running, while both area and pressure vary in time.

Usually the regression rate is modelled using a power law, as shown in Eq. (2).

$$r = a\, p^n, \tag{2}$$

where p is the pressure, and a and n are empirical constants. Such model emphasizes the role of pressure on combustion kinetics. Since this property exert such influence on burn rate, our model gather static test data and atmospheric data on pressure to enhance regression modelling. Besides the pressure, the internal surface area is a source of fluctuations in mass flow rate. Therefore, an accurate modelling of this property can provide insights on the internal ballistics.

2. SURFACE MODELLING

The surface was modelled in a quasi-3D manner: the grain was assumed to be a prism. This approach allowed us to represent the grain geometry in a simplified yet accurate way. Due to it's prismatic characteristics, the propellant shape can be described as a 2D curve extruded along an axis perpendicular to the 2D plane. Such curve is fully described by the XY coordinates of the constituent points and the connectivity between them, as shown in Fig. 1(a).

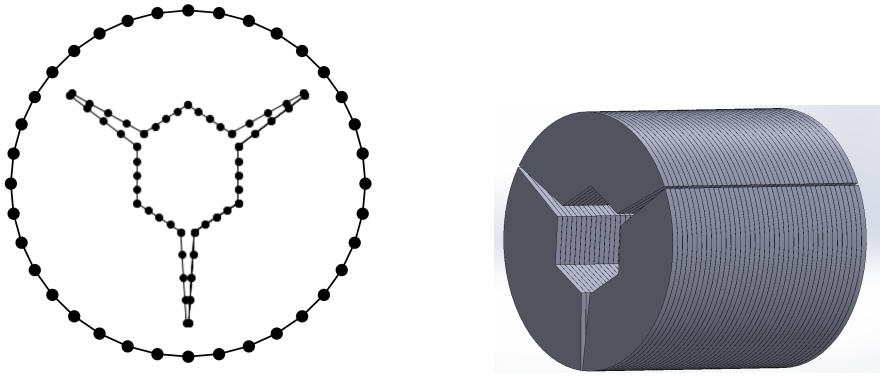

(a) (b)

Figure 1. (a) A 2D slice and it's determinant points. (b) A 3D propellant made from 2D slices.

This connectivity only occur in the 2D plane. The third dimension (along the propellant axis) is created through the stacking of many 2D planes. So, the 3D solid is described as a collection of 2D slices with similar burning behaviour, as shown in Fig. 1(b). For this simulations, the grain was divided in 100 slices.

3. SURFACE REGRESSION

3.1 Surface evolution

The regression of the 2D slice is done through the displacement of the curve surface, in a front-tracking manner. Such approach is similar to those in (Saintout *et al.*, 1989) and (Gueyffier *et al.*, 2015), which also used a similar Lagrangian displacement strategy.

During a timestep, each point is displaced according to Eq. (3). There are 3 informations required: the base point b_i, the burn rate r as predicted by Eq. (2) and the normal unitary vector $\mathbf{n}$. The base point is acquired through interpolation. It is chosen by adjusting a quadratic curve on 3 points in a way that the curve has the same area as the straight lines of the mesh. To achieve this curve, the parabola needs to pass through the base point defined as in Eq. (4). The points involved in this calculation are shown in Fig. 2.

$$\mathbf{p}_i^{t+1} = \mathbf{b}_i + r \cdot \mathbf{n} \tag{3}$$

$$\mathbf{b}_i = \mathbf{c}_i + 0.75 \cdot (\mathbf{p}_i - \mathbf{c}_i) \tag{4}$$

$$\mathbf{c}_i = 0.5 \cdot (\mathbf{p}_{i-1} - \mathbf{p}_{i+1}) \tag{5}$$

$$\mathbf{d}_i = [y_{i-1} - y_{i+1}, -x_{i-1} + x_{i+1}] \tag{6}$$

$$\mathbf{n}_i = \mathbf{d}_i / \|\mathbf{d}_i\| \tag{7}$$

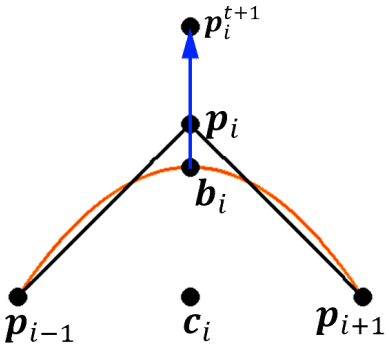

Figure 2. Interpolation and displacement scheme. The orange curve is a parabola fitted in a way that minimize the area between it and the mesh (black segments). The blue vector is the displacement $r \cdot \mathbf{n}$.

In order to find the correct direction to displace each point, the first step is to calculate the normal vectors of the burning surface. This is done as in Eq. (6), where x and y are the mesh points coordinates. The direction is then normalized in Eq. (7) to get a unitary vector. The equations 3 to 7 are applied to each mesh point and then the timestep properties are evaluated.

The internal area is obtained by calculating the slice perimeter and multiplying it by the slice length. This surface is then used to calculate the volume of the slice and it's mass. The loop runs until the slice mass reaches zero, and the main output is a curve showing how the slice mass declines during the burn. The derivative of the mass vs time curve is calculated to find $\dot{m}_f(t)$ and can be seen in Fig. 7. To test the algorithm three geometries were chosen: "circular", "circular with slots" and "flower", as in Fig. 3.

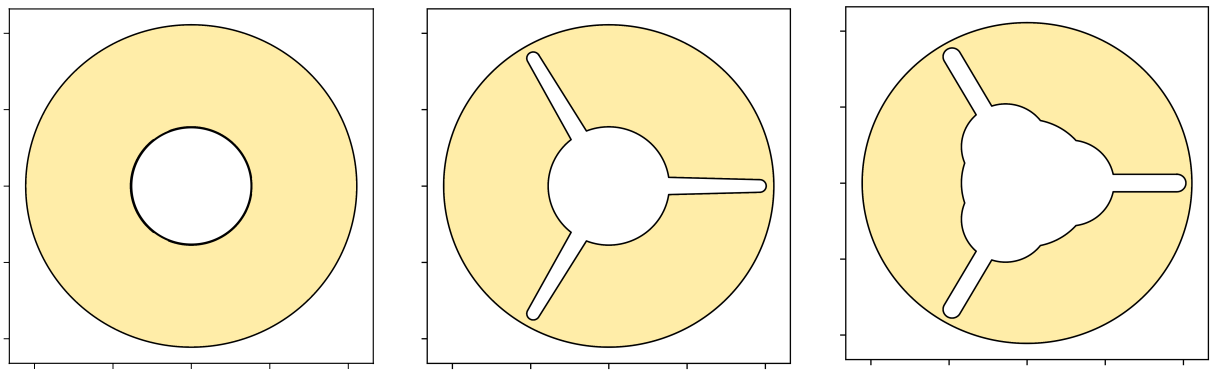

(a) (b) (c)

Figure 3. The 3 grain geometries modelled. (a) Circular geometry. (b) Circular with slots. (c) Flower.

3.2 Correcting issues

An issue that can arise is the interlapping of mesh points. This is prevented by measuring the angle between the surface normals, which is done computationally by taking the dot product of these vectors. When such product is positive, the angle between edges is greater than 90 degrees, indicating a smooth surface. When such product is negative the surface is very sharp and the vertex point is deleted to smooth the mesh. Such behaviour is shown in Fig. 4.

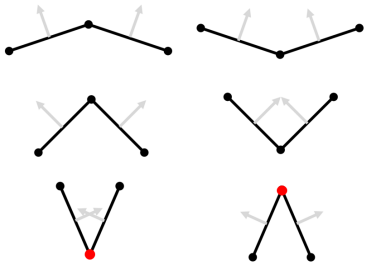

Figure 4. Top row: smooth mesh in normal conditions. The angle between edges is greater than 90 degree. Middle row: limit case. The dot product between normals is zero, implying perpendicular edges. Bottom row: the surface is very sharp, so a point is marked for deletion.

Another problem is the clustering of points. As the mesh evolves, some regions acquire a high density of points (which can result in numerical error) and other very low density (leading to loss of precision). To circumvent this issue, the 2D surface is parameterized by it's length and the points are rearranged according to a homogeneous distribution, preventing the clustering. This is shown in Fig. 5.

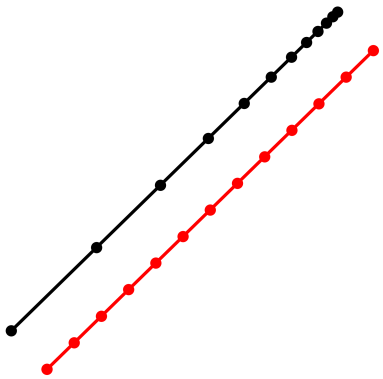

Figure 5. Mesh region before and after smoothing. The black mesh has a non homogeneous point distribution, while the red mesh is homogeneous but maintaining the same number of points.

4. FROM 2D TO 3D: MODELLING THE TRANSIENT

In a first attempt to model the burn, the working hypothesis was that the internal surface ignition was so fast that it could be modelled as instantaneous. So, to acquire the full grain's $\dot{m}(t)$ it was needed just to multiply the slice's $\dot{m}(t)$ by the number of slices. However, such approach delivered unrealistic high peak mass output, quicker than expected time of burn and a non-physical discontinuity at the beginning of the curve, contrasting with experimental findings. Therefore, introducing a delay to represent the fast-yet-finite required time to ignite the grain surface allowed us to model the expected transient behaviour. This fine-tuning in ignition is described by the ignition functions, which answers the question "how much time does it takes the slice at position X to starts burning?". Such functions are built following the restraints present in Table 1. The functions designed to meet these criteria are expressed in Eq. (8) and can be seen for many values of j in Fig. 6.

Table 1. Ignition Delay Functions requirements

Requirement	**Physical meaning**
The function must start at zero	the ignition has a point-source start
The function's inverse must have a null derivative at the end	the ignition stops smoothly
The function must monotonically increase	there are no "jumps" in the grain's ignition

$$A(x) = t_{Max}\left(\frac{\pi - \cos^{-1}\left(\frac{2x}{L} - 1\right)}{\pi}\right)^{j} \tag{8}$$

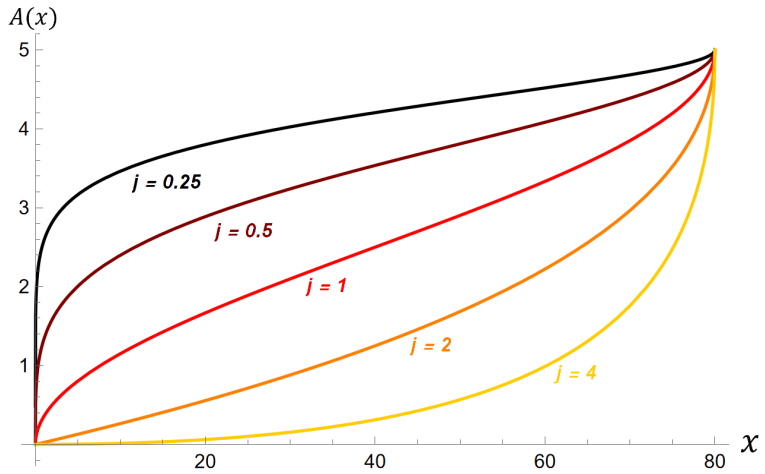

Figure 6. Ignition delay functions for many values of j. In this graph $tMax = 5$ and $L = 80$.

Using several values for j allow us to fit the grain $\dot{m}(t)$ to those achieved experimentally. For small j the ignition becomes instantaneous, while for large j it is delayed. $j = 1$ produces an almost linear ignition propagation. $\dot{m}_f(t)$ represent how $\dot{m}(t)$ of a single slice changes during time and can be seen in Fig. 7. To better understand how the burning behaviour of a single 2D slice reflects on the 3D grain, we need to investigate how all the slices are ignited and how this affect the propellant's $\dot{m}(t)$ curve.

The grain's $\dot{m}(t)$ is a summation of all slice's $\dot{m}_f(t)$. Since each slice at position x takes $A(x)$ seconds to ignite, the total grain $\dot{m}(t)$ is represented as a sum of $\dot{m}_f(t)$ with a time shift given by $A(x)$ as in Eq. (9). In this equation dL is the length of a single slice. $\dot{m}_f(t)$ has a time domain $t \in [0, t_{burn}]$. If the argument of function $A(x)$ falls outside the range of $\dot{m}_f(t)$ then $\dot{m}_f(t)$ is assumed to be zero at that slice. The physical meaning is that in a time argument smaller than 0 the slice still isn't ignited and with an argument larger than t_{burn} the slice already burned totally.

$$\dot{m}(t) = \sum_{i=0}^{nSlices} \dot{m}_f(t - A(i \cdot dL)) \tag{9}$$

5. RESULTS

To minimize the influence of other factors besides geometry, all grain lengths were kept the same, as well as the external diameter and burn rate. The main variables were the internal geometry itself and the ignition delay profile.

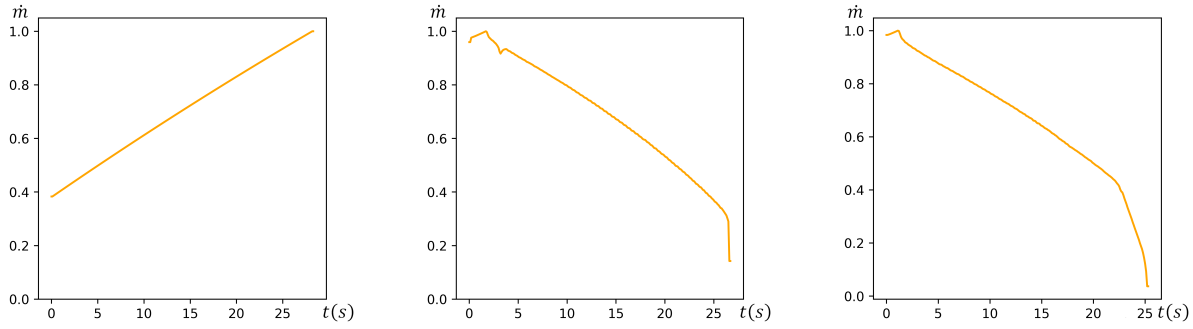

(a) (b) (c)

Figure 7. Slice normalized $\dot{m}_f(t)$ vs t curve. (a) Circular geometry. (b) Circular with slots geometry. (c) Flower geometry.

Several static tests were carried on to confront the model with real-world data. In order to acquire the data, an experimental apparatus was built and modelled as detailed in a previously published work (Pinheiro *et al.*, 2020). In short, the static test bench is comprised of a cylindrical combustion chamber attached to a sliding table. Such combustion chamber is equipped with an absolute pressure transducer and a load cell. These sensors are connected to a NI-9219 A/D module, from NI®, and the acquired data (pressure and thrust) is stored in a computer using an in-house software for data processing. The mass flow is evaluated from the pressure and thrust data using Eq. (10), where P_c is the measured chamber pressure, P_t the local atmospheric pressure, A_t the base bleed throat area and k the specific heat ratio.

$$\dot{m} = \frac{\left(\frac{P_c}{P_t}\right)^{1/k}\left(\left(\frac{P_c}{P_t}\right)^{\frac{k-1}{k}} - 1\right)(2kA_tP_c)}{k-1} \tag{10}$$

An example of the results obtained through this experimental setup is shown in Fig. 8. Figure 9 displays the curves calculated by the procedure described in sections 3 and 4.

The mass flow curves acquired in static tests using the “flower" and “circular with slots" geometries, as seen in Fig. 8, show resemblance to the calculated ones. The circular geometry was tested as a benchmark, and it produced a crescent mass flow profile, as expected. The circular slotted geometry and flower showed a similar patern of early peaking and then decreasing the flow, with a sharper decrease in the end of burn.

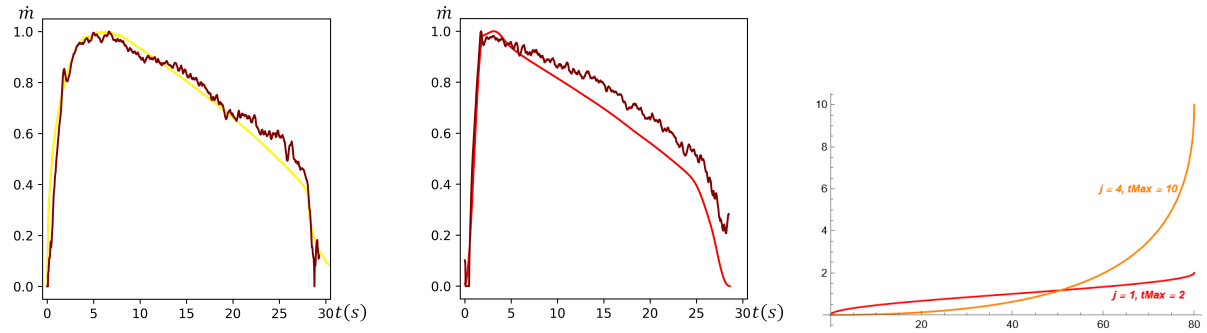

(a) (b) (c)

Figure 8. $\dot{m}(t)$ obtained from static tests against the best fit from simulations and ignition delay functions (a) Circular with slots. Best fit: $tMax = 10$ and $j = 4$. (b) flower. Best fit: $tMax = 2$ and $j = 2$. (c) Ignition delay functions used in the fits.

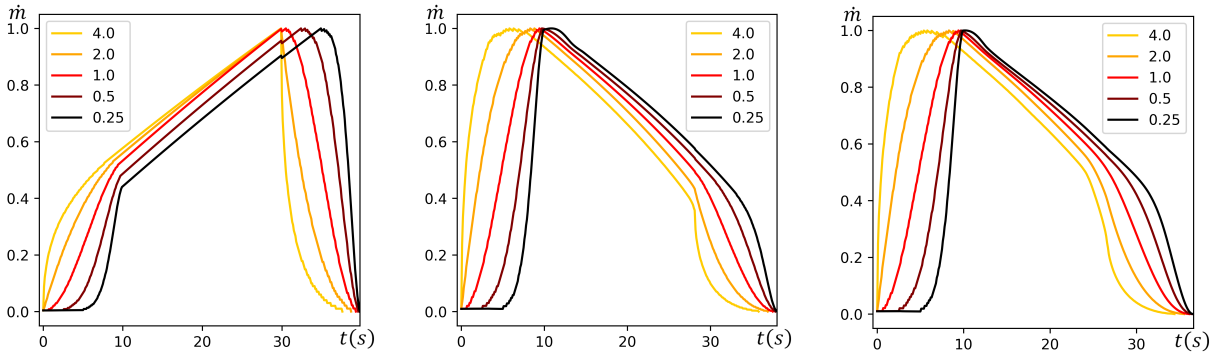

(a) (b) (c)

Figure 9. Normalized $\dot{m}$ vs t curves obtained from computer simulations using $tMax = 10$. (a) Circular geometry. (b) Circular with slots geometry. (c) Flower geometry.

According to Fig. 9, the presence of slots in the grain resulted in a decrescent profile instead of the crescent one present in the circular geometry. It can be seen that the ignition profile has a great influence on the curve shape, shifting the peak mass flow by several seconds. Such finding can directly impact the projectile trajectory behaviour, as seen in (Lucena *et al.*, 2020), (Lemos *et al.*, 2017) and (Lemos *et al.*, 2022).

After fitting the simulations, great agreement was found at the transient and peak stages of the burn. The slightly divergence between the test and simulated cruves after the peak is hypothesized to be due the fact that the mass flow out of the grain (simulated in this work) and the mass flow out of the chamber (measured in the static tests) show some differences as a result of effects of internal chamber ballistics: pressure build-up and a delay in expelling the gases. Such dynamic will be the focus in future investigations. The lack of a model for inside-chamber pressure made the model unable to produce the oscilations present in the experimental curve. Instead, it produced smooth curves. Even with this divergence, the curves shape still show great agreement, with a near constant decrescent shape after the peak and a sharper decrease near the end of burning.

6. CONCLUSIONS

A geometric model was built to model the mass flow of the base bleed system. The main idea was to use the grain volume variation as a measure of the mass being burned. This approach was made for a single grain slice, and a math-

ematical formulation for the ignition pattern allowed us to extend the 2D simulation results to the 3D grain. The results show great agreement in the transient phase and the peak stage, with very low computational cost. It is expected that a future work modelling the chamber pressure can reproduce the oscillations and increase the match between simulated and measured curves.

7. ACKNOWLEDGEMENTS

The authors thank FAPERJ (Research Support Foundation of the State of Rio de Janeiro), CNPq (National Council for Scientific and Technological Research), and CAPES (Coordination for the Improvement of Higher Education Personnel) for their financial support.

8. REFERENCES

Gueyffier, D., Roux, F., Fabignon, Y., Chaineray, G., Lupoglazoff, N., Vuillot, F., Hijlkema, J. and Alauzet, F., 2015. "Accurate computation of grain burning coupled with flow simulation in rocket chamber". *Journal of Propulsion and Power*, Vol. 31, No. 6, pp. 1761–1776.

Lemos, M.F., Amaral, P.S.T., Miceli, A., Silva-Junior, L.J. and Souza, E., 2017. "Development of national base bleed propellant grain applied for extended range ammunition". *Pesquisa Naval (SDM)*, Vol. 29, pp. 49–58.

Lemos, M.F., Lucena, R., Pinheiro, G.R.V., Mangiavacchi, N., Chalhub, D.J.N.M., Neubarth, L.A., Amaral, P.S.T., Silva-Junior, L.J., Ferreira, W.K.O. and Pinto, R.C., 2022. "From bench to shooting range: Correlating base bleed chemistry with the ballistic performance of extended range munition". In *International Symposium on Ballistics*. Vol. 2.

Lucena, R., Pinheiro, G.R.V., Mangiavacchi, N., Pontes, J., Chalhub, D.J.N.M., da Silva, W.R.R., Neubarth, L.A., Lemos, M.F., Amaral, P.S.T. and Silva-Junior, L.J., 2020. "Numerical aerodynamic simulation of an artillery projectile with a base bleed system". In *18th Brazilian Congress of Thermal Sciences and Engineering, ENCIT 2020 (Online)*.

Pinheiro, G.R.V., Lucena, R., Mangiavacchi, N., Pontes, J., Chalhub, D.J.N.M., da Silva, W.R.R., Neubarth, L.A., Lemos, M.F., Amaral, P.S.T. and Silva-Junior, L.J., 2020. "Simulation and static tests of base bleed gas generators". In *18th Brazilian Congress of Thermal Sciences and Engineering, ENCIT 2020 (Online)*.

Saintout, E., Le Roux, A., Ribereau, D. and Perrin, P., 1989. "Elea-a tool for 3d surface regression analysis in propellant grains". In *25th Joint propulsion conference*. p. 2782.

Sutton, G.P. and Biblarz, O., 2016. *Rocket propulsion elements*. John Wiley & Sons.

9. RESPONSIBILITY NOTICE

The authors are solely responsible for the printed material included in this paper.